Geomechanics and Engineering, *Vol. 27, No. 4 (2021) 405-417*
https://doi.org/10.12989/gae.2021.27.4.405

An efficient approach for stability analysis of rock slopes subjected to a transient drawdown

Yining Hu[1a], Ying Ding[2b] and Zhibin Sun*[2]

[1]*School of Civil Engineering and Transportation, Hohai University, Nanjing, China*
[2]*School of Automotive and Transportation Engineering, Hefei University of Technology, Hefei, China*

(Received November 14, 2020, Revised September 2, 2021, Accepted October 5, 2021)

Abstract. Since the water drawdown in a reservoir easily triggers the instability of a nearby slope, chart research on slopes that are subjected to drawdown conditions has attracted extensive attention recently. However, most studies only consider the extreme 'rapid/slow' drawdown conditions and ignore the general 'transient' drawdown scenario. This paper proposes an efficient approach for stability analysis of rock slope subjected to a transient flow, and provide a chart study and a parametric analysis. To address the challenge of determining the bent phreatic surface in a transient flow and to employ the nonlinear Hoek-Brown criterion of rock masses, a phreatic equation was adopted in this paper, together with the discretization technique. In the framework of limit analysis, the external work rate and the internal energy dissipation rate were computed. A calculation flow was proposed for capturing the optimized factor of safety (*FOS*) based on the strength reduction technique. Then, following the evaluation of this approach, a set of stability charts and an application example were presented. A parametric analysis was conducted to evaluate the influences of the rock properties and the hydrodynamic parameters on the factor of safety.

Keywords: Hoek-Brown failure criterion; limit analysis; stability charts; transient flow; water drawdown

1. Introduction

Slope stability is a classical problem in soil mechanics and practical engineering but also continuously attracts attention or research effect (Lysandros *et al.* 2020, Karray *et al.* 2018, Khorasani *et al.* 2019). Reservoir slopes are vulnerable under decreasing water levels of reservoirs (Gaziev 2001). To accurately evaluate the stability of reservoir slopes, many efforts have been made. For an extremely slow or rapid water drawdown case, Lane and Griffiths (2000) used the finite element method to develop stability charts that consider complex geometries and material properties. Viratjandr and Michalowski (2006) employed the limit analysis method to propose a series of stability charts for slope design. In these studies, the water table within a slope is postulated as a horizontal phreatic line during the drawdown process. Although this assumption is convenient for determining the pore pressure, it is only valid under extreme slow/rapid drawdown conditions. In more typical scenarios, the water level of reservoirs declines with a moderate ratio, and a strong bending of the phreatic line is observed, as shown in Fig. 1(b). The water surface that is obtained under the assumption may be unreliable and cannot be used to accurately represent the shape of the phreatic line. Therefore, it is necessary to develop a stability analysis approach for slopes that are subjected to a transient flow.

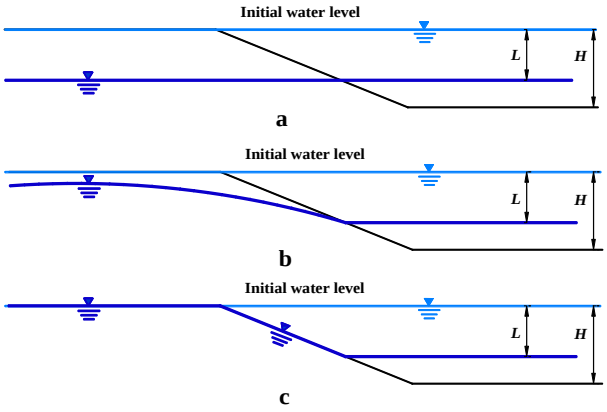

Fig. 1 Phreatic level after drawdown:(a)slow drawdown (b)rapid drawdown (c)transient drawdown

Due to the benefits of the application of commercial software, the numerical simulation method has become a useful tool for analyzing the patterns of phreatic lines (Carranza-Torres and Fairhurst 1999). Although meaningful conclusions have been drawn, this approach has the disadvantages of complicated modeling and a time-consuming process. To obtain results for a wide range of parameters, scholars have utilized a theoretical approach to analyze soil slope (Zheng *et al.* 2004). However, little attention has been paid to the stability of rock slopes under a transient flow. Therefore, a theoretical approach for rock slopes is still required. This paper proposes a method for the

*Corresponding author, Professor
E-mail: sunzb@hfut.edu.cn
[a] M.Sc. Student
E-mail: yh10n19@soton.ac.uk
[b] M.Sc. Student
E-mail: 17544932799@qq.com

ISSN: 2005-307X (Print), 2092-6219 (Online)

evaluation of a rock slope under transient drawdown conditions. In addition, the aforementioned studies used the linear Mohr-Coulomb (MC) criterion to describe the shear strength of soils. However, the MC criterion is unsuitable for analyzing the rock slope since most rocks have shear strength that varies nonlinearly with confining stress due to discontinuities in the rock mass (Merifiield *et al.* 2006, Tiwari and Latha 2017, Ukritchon and Keawsawasvong 2018). To address this problem, this study employs the nonlinear Hoek-Brown failure criterion within the framework of limit analysis. Furthermore, since the direct introduction of the phreatic line equation into the traditional limit analysis will inevitably result in a complicated integration operation (Viratjandr and Michalowski 2006, Saada 2012), a recently proposed discretization technique is used in this study. This technique innovatively utilizes a discretized sliding surface in the failure mechanism and has exhibited efficiency and flexibility on stability problems (Mollon *et al.* 2011, Alhajj Chehade *et al.* 2019).

The remainder of this paper is organized as follows: A discretization mechanism for a rock slope under a transient flow was introduced, and the energy dissipation of the rock mass and the external work rates due to gravity and the pore water pressure were derived. Next, the calculation framework of the safety factor was proposed, an optimization code was developed, and the performance of the phreatic equation and proposed approach was evaluated against the previous results. Eventually, a set of stability charts was provided for preliminary design, which is followed by a parametric analysis to explore the effects of the slope geometry and the hydraulic condition on the slope stability under a transient flow.

2. Limit analysis of slopes subjected to water drawdown

2.1 Phreatic surface in slope under drawdown conditions

A reservoir slope that is subjected to drawdown conditions is schematically presented in Fig. 2. Initially, the phreatic surface within the slope is horizontal to the level of the water table in the reservoir. When the water table declines from the height of $h_{0,0}$ to $h_{0,t}$ at moment t, the phreatic line also shows a downward trend and bends.

To provide an accurate mathematical description of the phreatic line, a function in the coordinate system shown in Fig. 2 is introduced. The following derivation is based on two assumptions: the aquifer is homogeneous and isotropic with infinite lateral extension, and the water level decreases at a constant rate v.

A differential equation of the unsteady seepage, which is on the Boussinesq equation, is expressed as

$$\frac{\partial h}{\partial t}=\frac{k}{\mu}\frac{\partial}{\partial x}\left(H_0\frac{\partial h}{\partial x}\right) \tag{1}$$

where x and h are the two coordinate axes of the coordinate system, as shown in Fig. 2; k is the permeability coefficient; μ is the specific yield; t is the duration of the water drawdown process; and H_0 is the aquifer thickness.

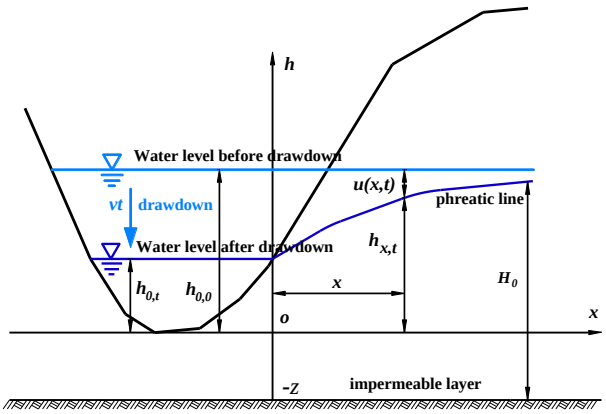

Fig. 2 Calculation sketch of phreatic line

For simplification, the parameter H_0 is approximated as a constant and replaced by the average thickness of the phreatic flow h_m. Then, the new equations are expressed as:

$$\frac{\partial h}{\partial t}=a\frac{\partial^2 h}{\partial x^2} \tag{2}$$

where $a=\frac{kh_m}{\mu}$

In consideration of the boundary conditions in Eq. (3) and via the use of mathematical techniques such as the Laplace transform and least-square fitting, a simplified formula for the phreatic line is derived, which is presented as Eq. (4). Details of the derivation can be found in the literature (Zheng *et al.* 2004).

$$\begin{aligned}&u(x,0)=0,0<x<\infty\\&u(0,t)=vt,t>0\\&u(\infty,t)=0,t>0\end{aligned} \tag{3}$$

$$h_{x,t}=\begin{cases}h_{0,0}-v(0.1091\lambda^4-0.7501\lambda^3\\+1.9283\lambda^2-2.2319\lambda+1)(0\le\lambda<2)\\h_{0,0}(\lambda\ge 2)\end{cases} \tag{4}$$

2.2 Pore-water pressure in the limit analysis

As it provides a strict upper bound on the actual limit loads, the kinematic approach of limit analysis is an effective approach for addressing the stability problem (Leshchinsky and Ambauen 2015, Bandini *et al.* 2003). Under the critical condition of a system, the rate of internal work D is equal to the rate of external forces W in any kinematically admissible field (Nadukuru and Michalowski 2013):

$$D=W \tag{5}$$

Typically, the rate of external forces W corresponds to the gravitational forces of the soil and rock. For slopes with a phreatic surface, the work rate of the pore water pressure W_u should be considered in the computational model, which includes the work rate of the pore pressure on the skeleton W_u' and the work rate of the water pressure on the

boundary $W_u^{''}$.

The first term, namely, W_u, is expressed as

$$W_u^{'} = -\int_V u v_i n_i dV \tag{6}$$

where u is the pore-water pressure, v_i is the velocity vector of the slope mass, n_i is the outward unit vector that is perpendicular to the submerged surface, and dV is the volume element.

The second term, namely, $W_u^{''}$, is expressed as

$$W_u^{''} = -\int_S p v_i n_i dS \tag{7}$$

where p is the water pressure that acts on the boundary of the slope under the water level and dS is the surface element. The work-energy balance equation can be expressed as

$$D = W_G + W_u^{'} + W_u^{''} \tag{8}$$

in which W_G is the work rate of gravity.

3. Application of the Hoek-Brown Failure Criterion

3.1 Generalized Hoek-Brown Failure Criterion

Experiments have demonstrated that the failure of a rock mass satisfies a nonlinear criterion. Hoek and Brown (2002) proposed the generalized Hoek-Brown failure criterion, which is expressed as follows:

$$\sigma_1 = \sigma_3 + \sigma_c\left(\frac{m\sigma_3}{\sigma_c} + s\right)^n \tag{9}$$

where σ_1 and σ_3 denote the maximum and minimum principal stresses, respectively; σ_c denotes the uniaxial compressive strength of the rock mass; and m, s, and n are dimensionless parameters, which are calculated via the following equations:

$$m = m_i\, exp\left(\frac{GSI - 100}{28 - 14D_0}\right) \tag{10}$$

$$s = exp\left(\frac{GSI - 100}{9 - 3D_0}\right) \tag{11}$$

$$n = \frac{1}{2} + \frac{1}{6}\left[exp\left(-\frac{GSI}{15}\right) - exp\left(\frac{-20}{3}\right)\right] \tag{12}$$

where GSI is the geological strength index that reflects the integrity of rock masses; D_0 is the disturbance factor, which ranges from 0 to 1.0; and m_i is an index that is related to the rock type.

3.2 Generalized Tangential Technique

The generalized tangential technique is a practical method for introducing the nonlinear Hoek-Brown failure criterion into the stability analysis of geotechnical structures (Huang and Yang 2010). Via the generalized tangential technique, the nonlinear curve is replaced by one of its tangent lines, and an optimization process is utilized to identify the optional tangent line that can produce the critical result. The tangent lines are expressed as

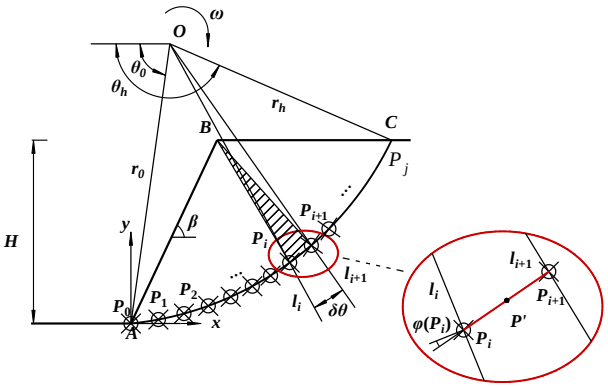

Fig. 3 Generation of a potential failure mechanism by 'point-to-point' method

$$\tau = c_t + \sigma_n \tan\varphi_t \tag{13}$$

where c_t and φ_t are the equivalent cohesion and the friction angle. In the computational process, φ_t is a parameter to be optimized. For the generalized Hoek-Brown failure criterion, the equivalent cohesion c_t is determined via the following equation:

$$\begin{aligned}\frac{c_t}{\sigma_n} = {} & \frac{\cos\varphi_t}{2}\left[\frac{mn(1-\sin\varphi_t)}{2\sin\varphi_t}\right]^{\frac{n}{1-n}} \\ & - \frac{\tan\varphi_t}{m}\left(1 + \frac{\sin\varphi_t}{n}\right)\left[\frac{mn(1-\sin\varphi_t)}{2\sin\varphi_t}\right]^{\frac{1}{1-n}} \\ & + \frac{s}{m}\tan\varphi_t\end{aligned} \tag{14}$$

4. Generation of the discretization mechanism

In kinematic analysis, a kinematically admissible failure mechanism is necessitated for reflecting the 'real' collapse velocity field. The shape features of the collapse mechanism are estimated in consideration of a pre-postulated slip surface. However, the traditional failure mechanisms that are expressed by analytic equations are not suitable for nonhomogeneous slopes. To overcome this shortcoming, a novel discretization failure technique was proposed recently (Sun *et al.* 2018). This technique also provides avenues for considering more complicated effects that cannot be readily resolved using the conventional method. Herein, the discretization technique is used to consider the pore-pressure pressure that is caused by the nonlinear phreatic surface.

The discretization mechanism is illustrated in Fig. 3. The slip surface contains a total of j+1 points. The generation of the slip surface starts from point P_0 (slope toe A), proceeds toward the slope crest BC, and terminates

at the intersection point P_j. The core strategy of the generation process lies in the 'point-to-point' technique, which generates point P_{i+1} by rotating a prespecified increment $\delta\theta$ from point P_i. The properties of segment line P_iP_{i+1} can be deemed homogeneous.

In consideration of the features of the shear failure of soils with internal friction angle φ, the direction of the shear surface has an angle of φ with the direction of the velocity, which is perpendicular to the rotation radius. A polar coordinate system is established with O as the origin point. According to the geometric relationship, the coordinates of the point P_{i+1} (x_{i+1}, y_{i+1}) can be determined via the following equation:

$$\begin{cases} x_{i+1} = x_i + \dfrac{\sqrt{(x_i - x_o)^2 + (y_i - y_o)^2} \times \sin\delta\theta}{\sin(\pi/2 + \varphi - \delta\theta)} \times \cos(\theta_i - \pi/2 + \varphi) \\ y_{i+1} = y_i + \dfrac{\sqrt{(x_i - x_o)^2 + (y_i - y_o)^2} \times \sin\delta\theta}{\sin(\pi/2 + \varphi - \delta\theta)} \times \sin(\theta_i - \pi/2 + \varphi) \end{cases} \tag{15}$$

where θ_i is the angle between the rotational radius OP_i and the horizontal line, x_o and y_o are the coordinates of the rotation center O, and $\delta\theta$ denotes the angle between two successive radius lines. Points are generated repeatedly until y_{i+1} is greater than or equal to the height of the slope. After connecting the two adjacent points from P_0 to P_j with straight lines, the whole collapse mechanism is realized.

Since the normality condition was included in the derivation of Eq. (15), the collapse mechanism satisfies the associated flow rule. Additionally, the pore pressure that is created by the nonstandard phreatic line can be conveniently considered with the discretization mechanism. Additional details will be provided in the next section.

5. Computation of the safety factor

Calculating the rates of external work and internal energy dissipation is an essential task in kinematic analysis. In the failure mechanism of a reservoir slope, the work rates consist of the rates of the weight of the collapsed block and the pore water pressure, and the energy dissipation comes from the plastic deformation along the slip surface.

The calculation of the external force rates is illustrated in Fig. 4. The sliding block is divided into many triangular elements, such as BP_iP_{i+1} in Fig. 4 (a). As a result, the gravitational work rates W_G can be obtained by summing the elementary work rates:

$$W_G = \sum W_{G_i} \tag{16}$$

where W_{Gi} is the work rate of gravity in the ith region, which can be calculated via the following equation:

$$W_{Gi} = \vec{G}_i \cdot \vec{v}_{Gi} = -\gamma\omega S_i R_{Gi} \cos\theta_{Gi} \tag{17}$$

where γ is the unit weight of the rock masses, S_i is the elementary area of BP_iP_{i+1}, R_{Gi} is the distance between the element barycenter P_{Gi} and the rotating center O, and θ_{Gi} is the angle between OP_{Gi} and the horizontal direction, as plotted in Fig. 4 (c).

As discussed earlier, the pore water pressure that affects

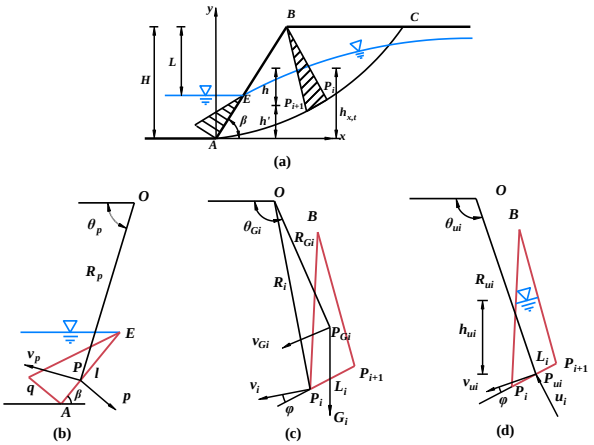

Fig. 4 Elementary analysis for calculation of work rate of water pressure within the slope

the slope can be categorized into two parts: the part within the slope mass and the part that occurs on the slope surface. According to the work of Michalowski (2006), the effect of the first part can be degraded by the external forces that are acting on the slip surface. As the slip surface is discrete, the work rates can be obtained via summation of the elementary work rates:

$$W_u^{'} = \sum W_{ui}^{'} \tag{18}$$

where $W_{ui}^{'}$ is the work rate of the pore pressure that is acting on segment P_iP_{i+1}.

Assuming that the pore pressure on segment P_iP_{i+1} is constant, $W_{ui}^{'}$ can be expressed as :

$$W_{ui}^{'} = -\omega\gamma_w h_{ui} R_{ui} \sin\varphi \tag{19}$$

where h_{ui} is the height of the water table at the midpoint of segment P_iP_{i+1}, γ_w is the unit weight of water, and R_{ui} is the distance between the midpoint P_{ui} and the rotating center O, as shown in Fig. 4(d).

The impact of the second part is equivalent to a triangularly distributed load since the value of the pore pressure increases linearly from point E to point A, as shown in Fig. 4(b). The distributed load is simplified as a point force. Thus, the work rate of this part of the pore pressure can be computed directly via the following equation:

$$W_u^{''} = \omega\gamma_w (H - L)^2 R_p \cos(\beta + \theta_p)/2 \sin\beta \tag{20}$$

where H is the height of the slope, L is the height of the falling water level, R_p is the distance between the rotating center O and the application point of the resultant force of the pore pressure, and θ_p is the angle between OP and the horizontal direction.

Accordingly, the total work rate of the pore pressure is the sum of these two components:

$$W_u = W_u^{'} + W_u^{''} \tag{21}$$

The overall rate of energy dissipation is calculated by summing the elementary rates:

$$D = c\omega \sum L_i R_i \cos\varphi \tag{22}$$

where L_i is the length of segment P_iP_{i+1} and R_i is the length of OP_i.

After obtaining the power rates, the safety factor of slopes can be obtained via the combination of the strength reducing method and the dichotomic approach. The calculation is described as a modification process for the reduction coefficient of the shear strength, with which the slope reaches a limit state. The computation process is detailed as follows:

Step A: Set the search range of the safety factor $[FOS_1,FOS_2]$.

Step B: Set $FOS=\frac{(FOS_1+FOS_2)}{2}$. Search $\min|W-D|$ for two independent variables r_0 and θ_0 with the shear strength cohesion=$\frac{c}{FOS}$ and the friction angle=$\frac{\tan\varphi}{FOS}$.

Step C: If $\min|W-D|>0$, set $FOS_2=FOS$. Otherwise, set $FOS_1=FOS$.

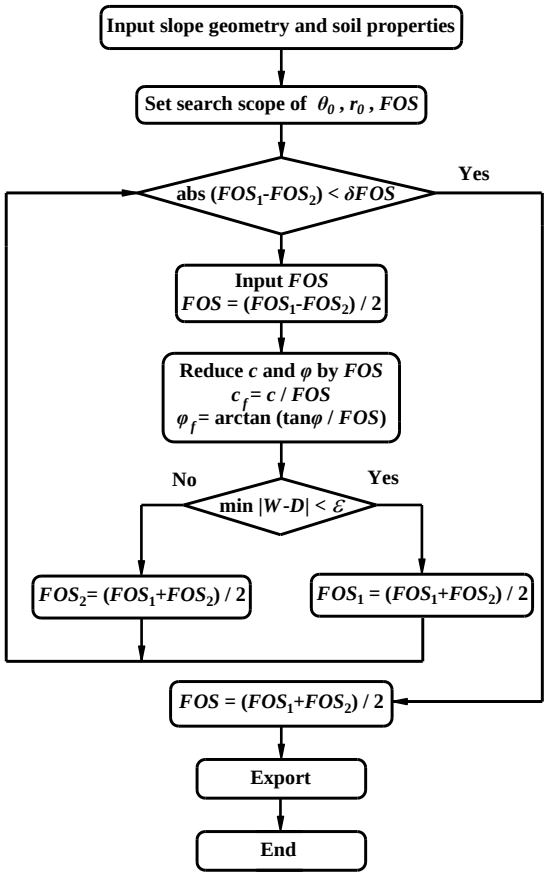

Fig. 5 The computation and optimization flow of the safety factor

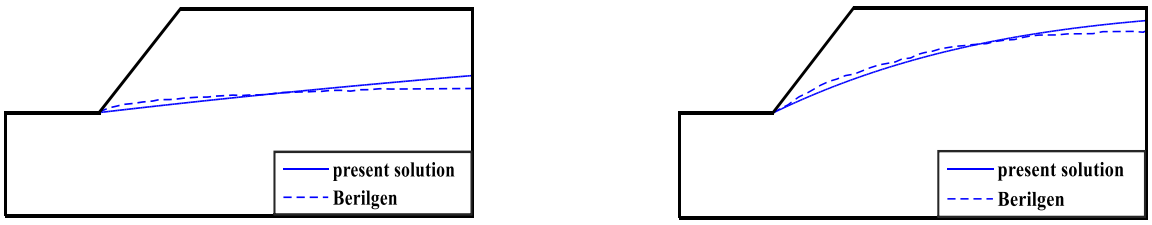

(a) v=1m/d, k=10^{-4}cm/s (b) v=0.1m/d, k=10^{-4}cm/s

Fig. 6 Comparison for phreatic line of present solution and Berilgen at ultimate rate L/H=1

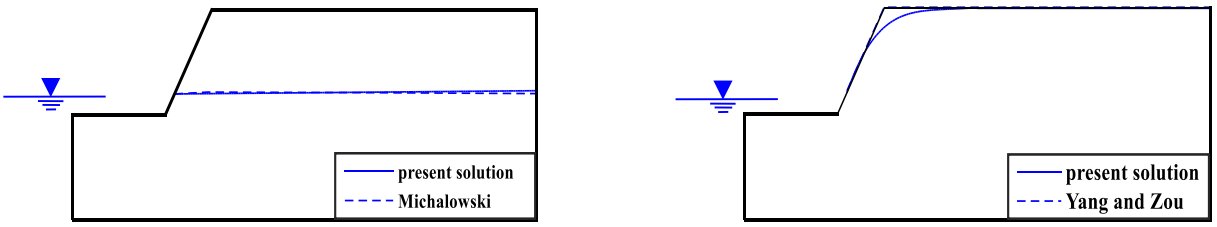

(a) v=10^{-4}m/d, k=10^{-4}cm/s (b) v=10^{4}m/d, k=10^{-4}cm/s

Fig. 7 Comparison for phreatic line of present solution: (a)slow flow; (b) rapid flow

Table 1 Comparison of safety factor with Berilgen (2006) for transient drawdown

v	k		L/H					
(m/d)	(cm/s)	Result	0	0.2	0.4	0.6	0.8	1.0
0.1	1×10^{-4}	Present solution	2.68	2.3109	1.9422	1.7409	1.6947	1.7434
0.1	1×10^{-4}	Berilgen	2.68	2.22	1.9	1.7	1.67	1.69
0.1	1×10^{-6}	Present solution	2.68	2.1641	1.6484	1.3516	1.1797	1.1172
0.1	1×10^{-6}	Berilgen	2.68	2.08	1.63	1.32	1.18	1.12
1	1×10^{-4}	Present solution	2.68	2.2422	1.7422	1.4453	1.2734	1.2266
1	1×10^{-4}	Berilgen	2.68	2.1	1.7	1.44	1.32	1.3
1	1×10^{-6}	Present solution	2.68	2.1484	1.6328	1.3203	1.1484	1.0859
1	1×10^{-6}	Berilgen	2.68	2.05	1.6	1.31	1.13	1.09

Table 2 Comparison with Yang and Zou (2006) for rapid drawdown: $r_u = 0.1$

β				GSI					
(°)	m_i	Result	Evaluating index	30	40	50	60	70	80
85	7	Present solution	Fs	1.0371	1.0371	1.0176	0.9885	0.9980	1.0166
85	7	Yang and Zou	Ns	0.79	0.93	1.06	1.19	1.31	1.42
85	15	Present solution	Fs	0.9876	0.9772	1.0172	1.0016	1.0391	0.9997
85	15	Yang and Zou	Ns	0.48	0.57	0.66	0.75	0.86	0.98
80	7	Present solution	Fs	0.9980	1.0371	1.0162	0.9885	1.0566	0.9980
80	7	Yang and Zou	Ns	1.31	1.31	1.45	1.57	1.68	1.77
80	15	Present solution	Fs	1.0234	0.9922	1.0159	0.9897	0.9953	0.9897
80	15	Yang and Zou	Ns	0.85	0.98	1.08	1.18	1.28	1.39
75	7	Present solution	Fs	0.9990	1.0176	0.9899	0.9980	1.0162	1.0057
75	7	Yang and Zou	Ns	1.64	1.84	1.98	2.08	2.16	2.21
75	15	Present solution	Fs	1.0234	0.9922	0.9922	0.9891	1.0391	1.0234
75	15	Yang and Zou	Ns	1.56	1.71	1.79	1.85	1.91	1.98

Step D: Repeat steps B and C until $(FOS_2 - FOS_1) < \delta FOS$, where d is the user-defined error.

6. Comparisons

In this section, comparisons are performed to explore the applicability of the phreatic line equation and the validity of the kinematic solution for the safety factor.

6.1 Validation of the phreatic surface equation

As described earlier, the phreatic line within a slope can be determined via numerical simulation. Berilgen (2006) used PLAXIS to investigate the flow-free surface of a soil slope while considering various drawdown rates. The numerical solutions were used to validate the theoretical results in this study. The basic input parameters are $H = 7m$, $k = 10^{-4}$cm/s, $v = 1m/d$, and $0.1m/d$, according to Berilgen's paper. The specific yield of $\mu = 0.01$ is specified by Younger and Elliot (1995), and the aquifer thickness of $z = 10m$ is obtained from the paper of Lu (2011).

Table 3 Comparison of safety factor with Viratjandr and Michalowski (2006) for slow drawdown: $r_u = 0.1$, slope 1:1

			L/H		
GSI	m_i	Result	0	0.4	1
10	7	Present solution	2.3900	1.8055	1.6490
10	7	Michalowski	2.45	1.90	1.86
10	15	Present solution	2.1929	1.6061	1.5060
10	15	Michalowski	2.20	1.78	1.65
30	7	Present solution	3.6565	2.0492	2.4729
30	7	Michalowski	3.75	2.30	2.65
30	15	Present solution	2.7629	2.6689	1.9098
30	15	Michalowski	2.95	2.80	2.18

According to Fig. 6, apart from minor differences, the results that were obtained in this study agree with those of Berilgen (2006), thereby substantiating the robustness of the proposed approach in both the rapid ($v = 1$m/d) and slow ($v = 0.1$m/d) drawdown regimes.

In addition, aside from the transient condition, the phreatic surface can also approach the water level in

extremely 'rapid' and 'slow' drawdown processes. The obtained and assumed water tables are plotted in Fig. 7.

6.2 Validation of the safety factor of the slope

The kinematic solutions of safety factors are compared with the previous results of Berilgen (2006) for a transient flow. For comprehensive comparison, the proposed approach is also evaluated for an extremely rapid/slow flow, in the comparison with the solutions of Yang and Zou (2006) (in which an extremely rapid flow is considered) and Viratjandr and Michalowski (2006) (in which an extremely slow flow is considered).

The soil that is governed by the Mohr-Coulomb criterion was analyzed in the study of Berilgen (2006), whereas the present study focuses on Hoek-Brown media. A necessary degradation is conducted to ensure that the code can cover the Mohr-Coulomb scenario. The results are compared in Table 1. The maximum discrepancy between the two solutions is less than 5%; hence, the proposed approach performs well under a transient condition. The error may come from the degradation algorithm and the optimization method.

Yang and Zou (2006) formulated the stability factor of a rock slope under rapid water drawdown via a combination of the generalized tangential technique and the log-spiral mechanism. According to the definition of the stability factor, when $c/(\gamma H)$ equals to stability factor, the slope is in critical state and the safety factor of the slope equals to 1.0. The stability factor of Yang and Zou and the corresponding safety factor from the proposed approach are listed in Table 2. The other parameters are $\sigma_c = 5$MPa, $\gamma = 25$ kN/m^3, $D_0 = 0$, $n = 0.5$, $\alpha = 0°$, and $r_u = 0.1$. The obtained safety factors are close to 1.0; hence, the proposed approach is reliable under the extremely rapid drawdown condition.

Michalowski (2006) provided the stability charts of a Mohr-Coulomb slope under the slow drawdown condition.

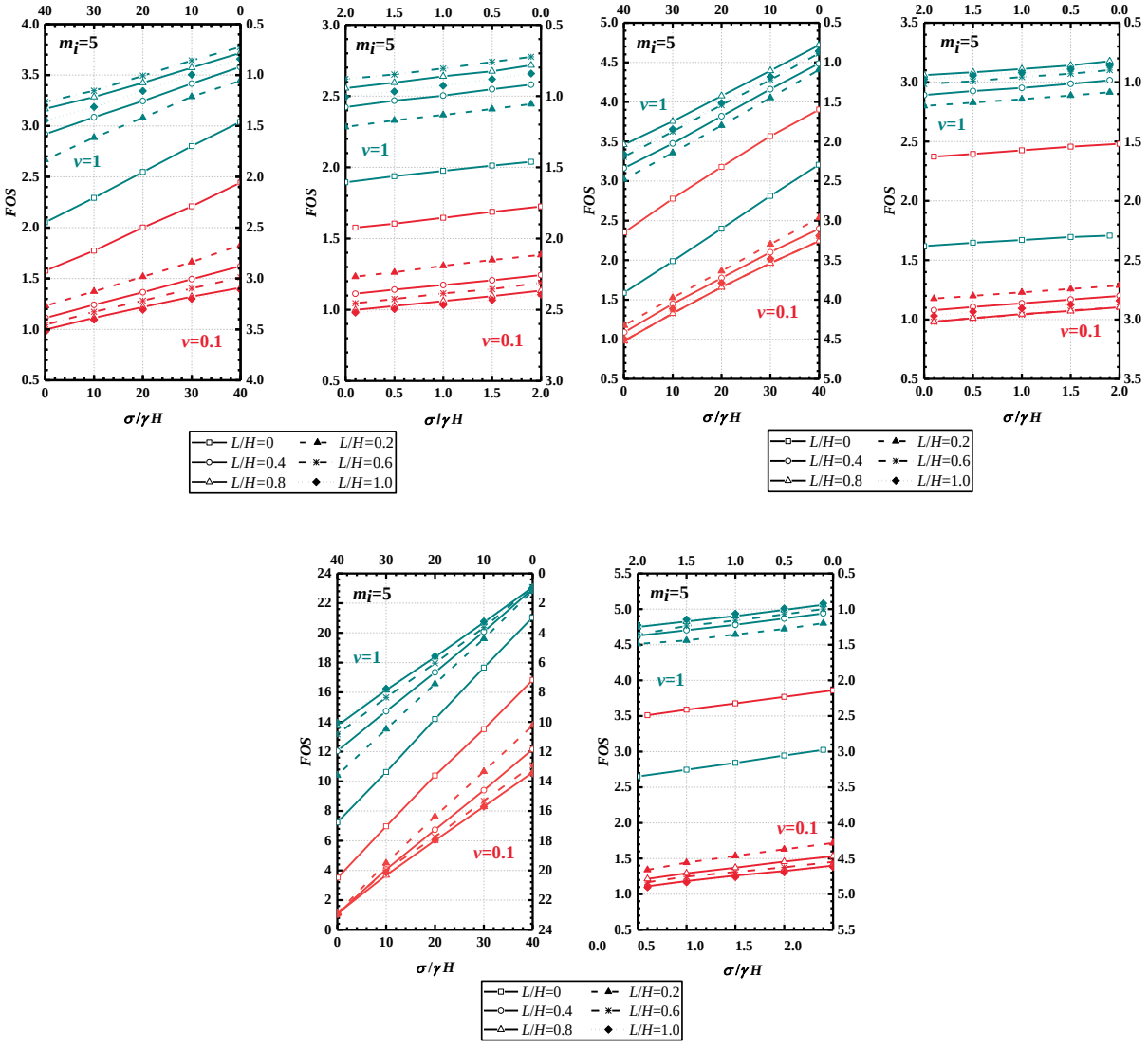

Fig. 8 Stability charts for $\beta = 45°, m_i = 5,$ GSI =10, 30, 70

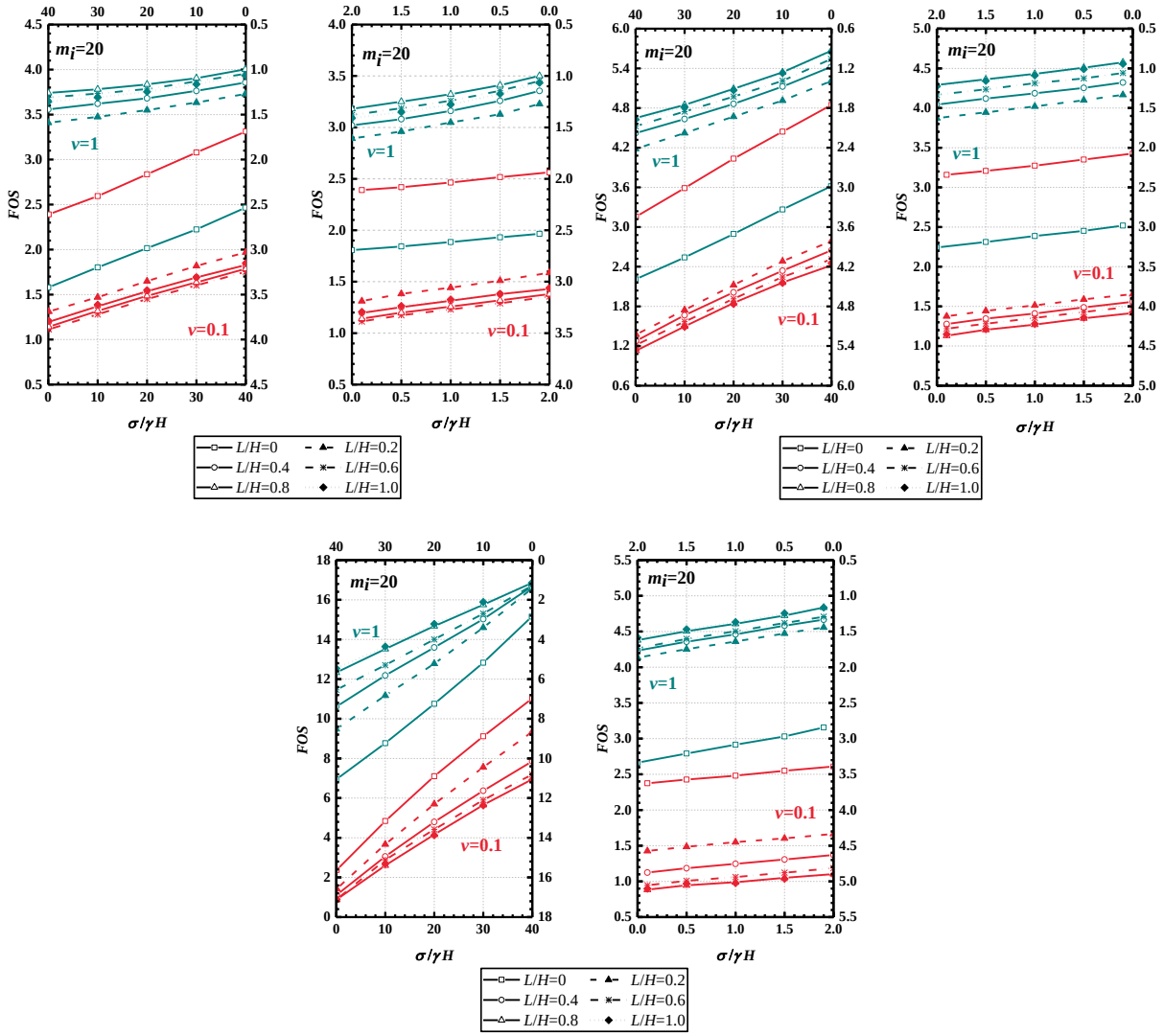

Fig. 9 Stability charts for $\beta = 45°, m_i = 20,$ GSI =10, 30, 70

This study also computed the safety factor via the equivalent parameter method; the results are listed in Table 3 with those of Michalowski (2006). The HB parameters are $D_0 = 0$, $m_i = 7$ and 15, and $GSI = 10$ and 30, and the slope inclinations are 1:1 and 1:2. In Table 3, satisfactory agreement is observed between the solutions of Michalowski and those of the current study, with a maximum discrepancy of less than 10%. The errors are attributed to the equivalent method.

According to the comparison results, the phreatic equation can describe a phreatic line that is close to a numerical result. With the application of the equation, the kinematic analysis can yield an accurate result.

7. Stability charts

Stability charts are widely used by engineers and designers to estimate the stability of slopes, especially for preliminary design purposes. Although many efforts have been contributed to the study of stability charts (Viratjandr and Michalowski 2006, Li *et al.* 2008), most were aimed at soil slopes that conform to the Mohr-Coulomb failure criterion. Chart research on rock slopes with a nonlinear failure criterion under a more general transient flow has not been fully developed. To provide a simple and comprehensive method for the stability evaluation of reservoir HB slopes, a series of charts is presented in this section.

Facilitated by the work of Carranza-Torres and Fairhurst (1999), it has been revealed that for HB rock slopes with specified indices GSI, m_i, and β, the safety factor FOS is only related to the magnitude of $SR = \sigma_{ci}/\gamma H$, where σ_{ci} is the uniaxial compressive strength of the intact rock. This correspondence between FOS and SR has been successfully applied to the chart research of rock slopes. Sahoo and Shukla (2019) have plotted a series of $SR - FOS$ charts for 2D and 3D rock slopes. Similarly, a stability analysis of rock slopes under transient drawdown conditions is conducted to provide a set of charts, as shown in Figs. 8 to 13.

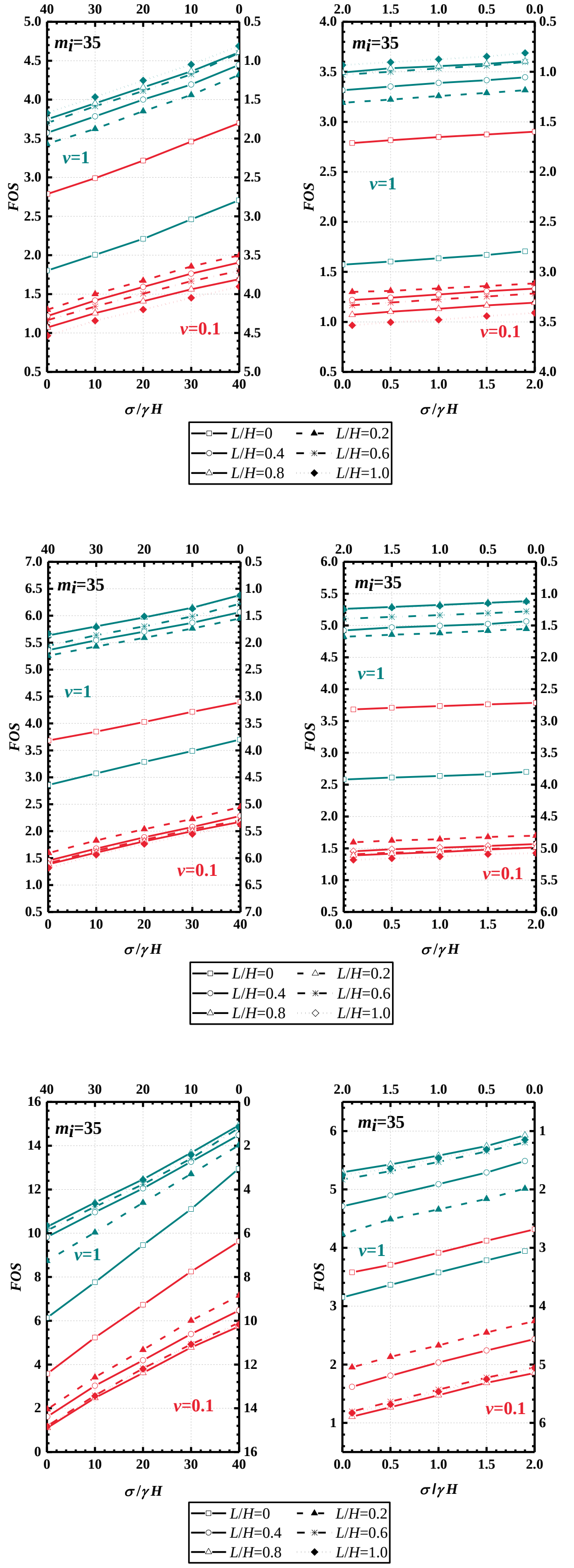

Fig. 10 Stability charts for $\beta = 45°, m_i = 35$, GSI =10, 30, 70

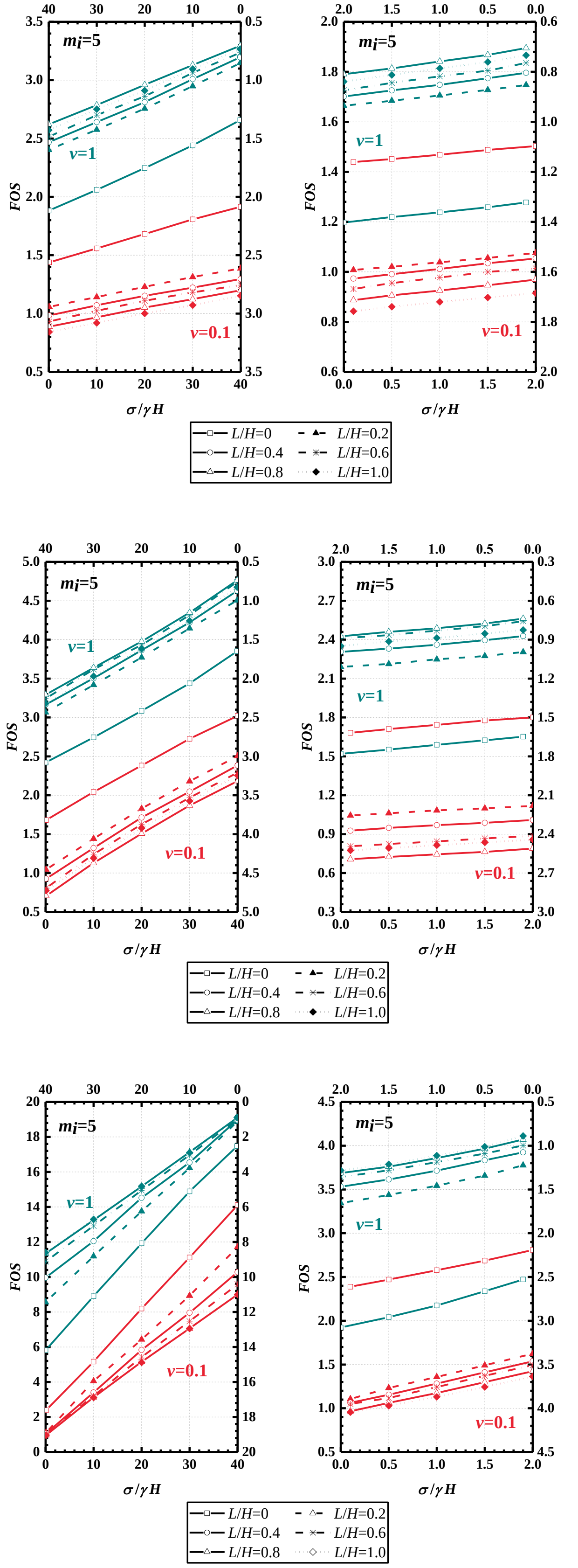

Fig. 11 Stability charts for $\beta = 60°, m_i = 5$, GSI =10, 30, 70

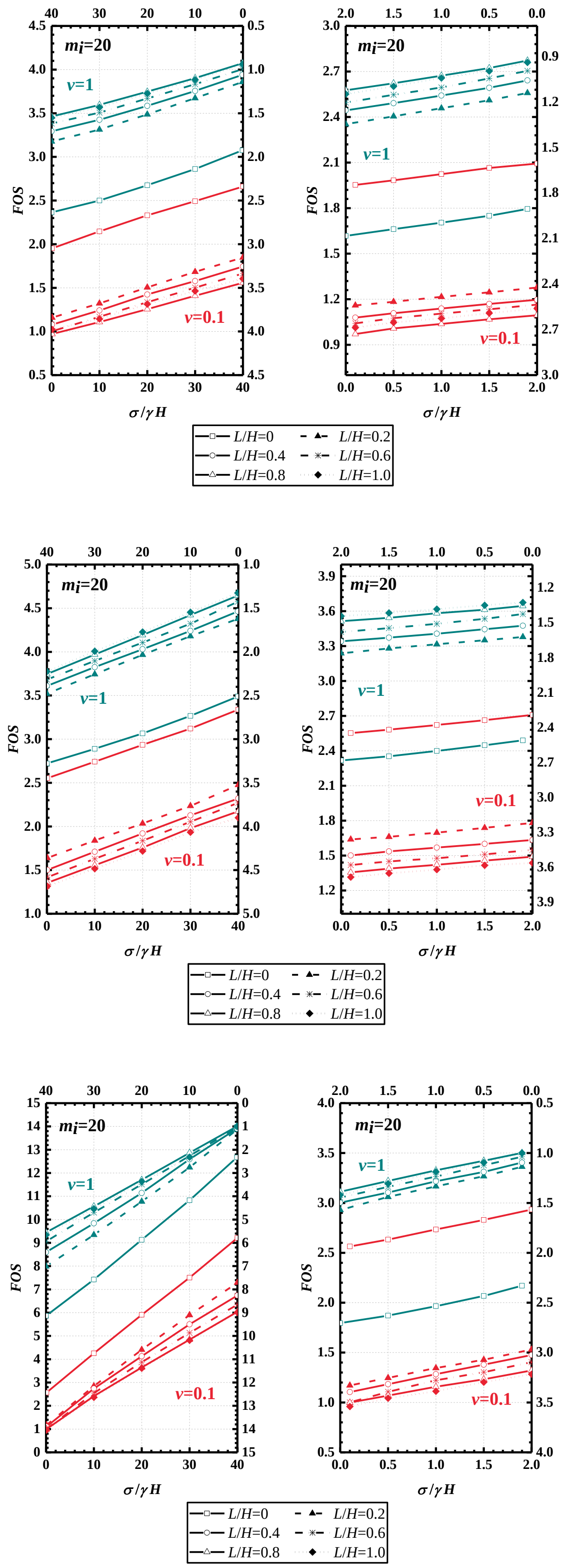

Fig. 12 Stability charts for $\beta = 60°, m_i = 20$, GSI =10, 30, 70

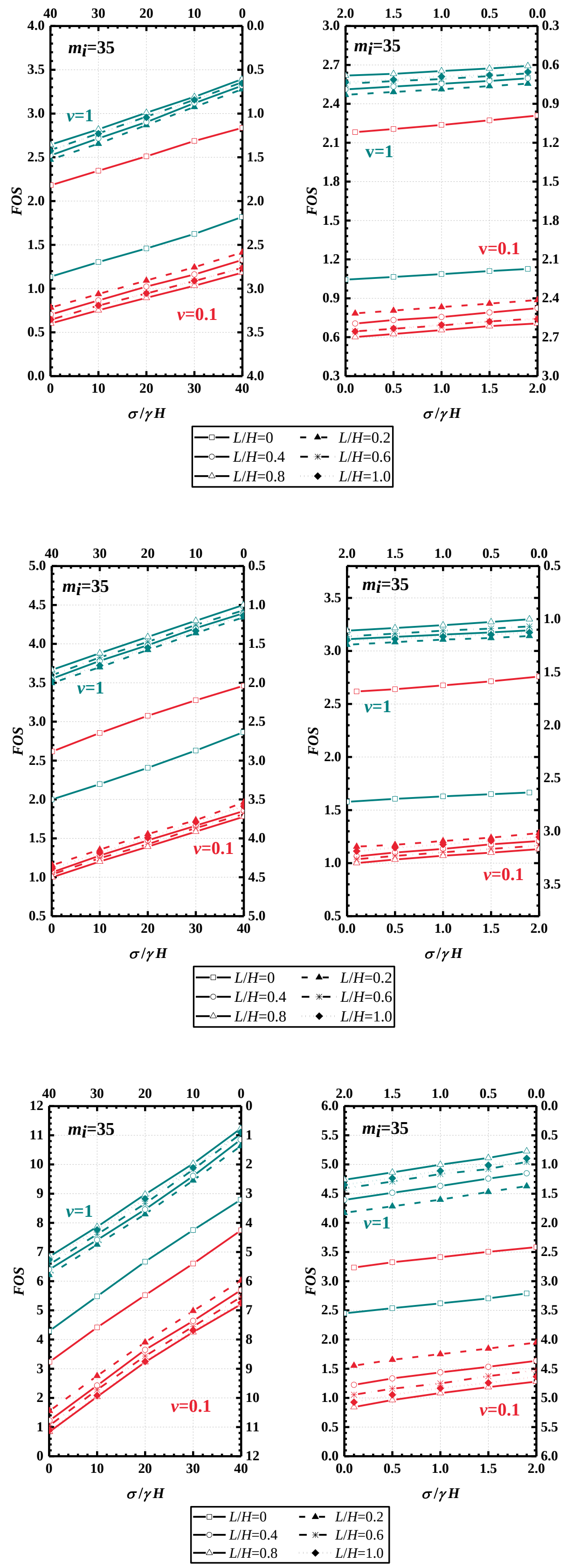

Fig. 13 Stability charts for $\beta = 60°, m_i = 35$, GSI =10, 30, 70

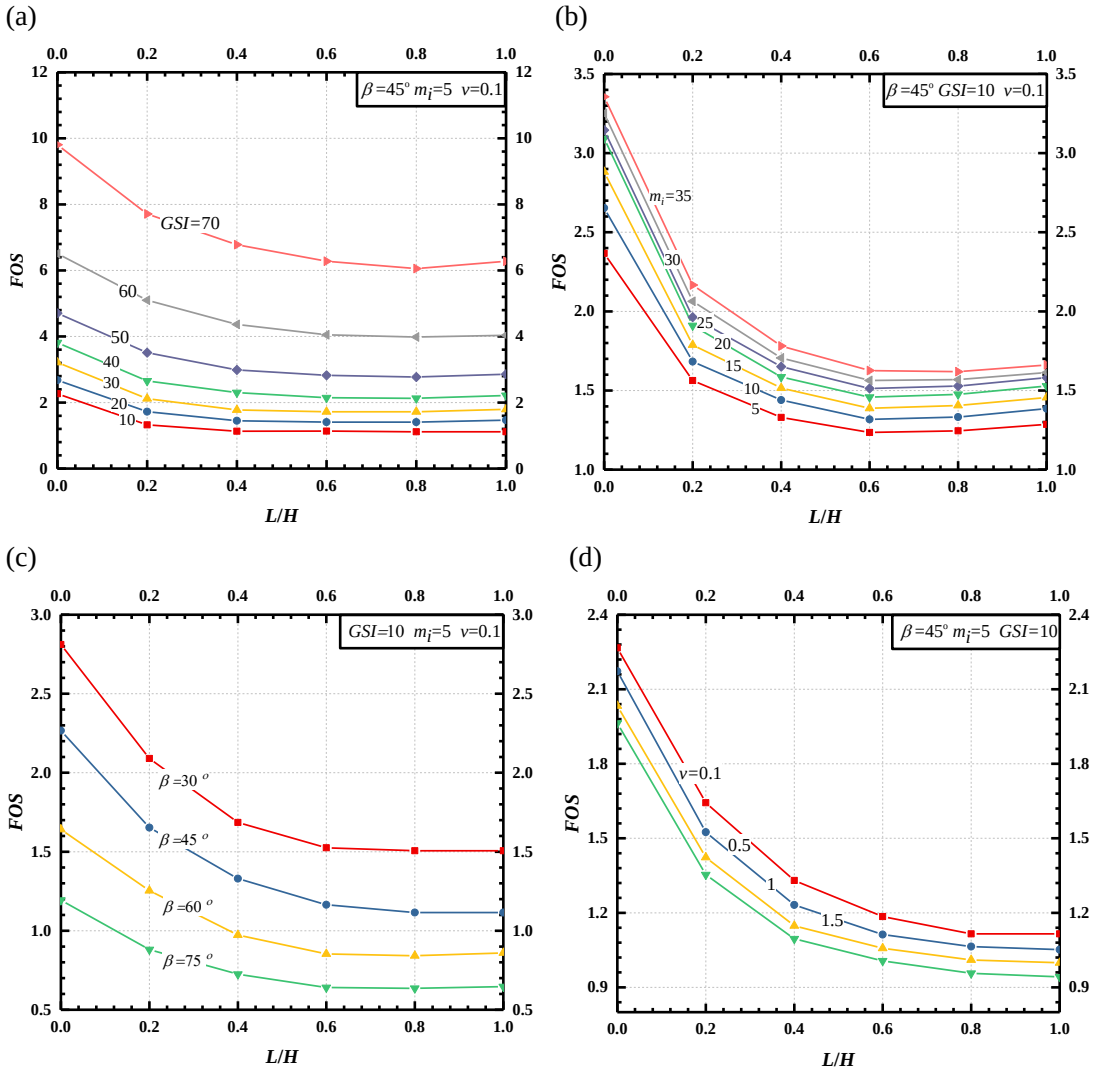

Fig. 14 Variation of safety factor at different values of $GSI, \beta,$ and v

For a wide range of applications, the parameter m_i is set to 5, 20 and 35 in the charts to cover the range from hard rock to soft rock. Meanwhile, we consider $GSI = 10$, 30 and 70 to include highly fractured rock and relative intact rock. Furthermore, all rock masses are assumed to be undisturbed, namely, $D_0 = 0$. Two rates of water drawdown are considered in these charts. The results for the relatively slow process with v = 0.1 m/d are represented by the green lines, and those for the process with v =1 m/d, which is more typical as a fast process (Berilgen 2006), are denoted by the red lines. The permeability parameter k is set to 0.08 m/d since the permeability of jointed rocks typically ranges from 10^{-13} to 10^{-9} m^2 (Rutqvist and Stephansson 2003). In addition, the height of the impermeable layer is 10 m and the specific yield is 0.01, according to previous studies (Younger and Elliot 1995) and the numerical simulation that was conducted in the previous section.

Fig. 8, 9, 10 plots the safety factor of the slope with the inclination of 1:1. Each curve in a chart represents the value of FOS at a specified ratio L/H, which is the water level coefficient. The value of SR ranges from 0 to 40. Moreover, separate charts for the range of SR 0-0.1 are provided.

According to Figs. 8-10 and Figs.11-13, the safety factor increases with the value of $\sigma/\gamma H$; hence, SR has a substantial positive impact on the slope stability.

Additionally, although according to most charts the slope stability steadily deteriorates with the fall of the water level, in several cases the minimum safety factor is attained before the reservoir has completely drained. This phenomenon is consistent with the result acquired by plane strain analysis of Lane and Griffiths (2000), which can be explained by the trade-off between the work rates of the external water pressure and the internal water pressure. Additional details can be found in the manuscripts of Lane and Griffiths (2000).

Figs.11-13 plots the safety factor of slopes with an inclination angle of 60°. The variations with the water level coefficient L/H and the parameters SR are similar to the case of $\beta = 45°$. In addition, the change of FOS with SR seems to be substantial under a relatively small value of m_i.

Based on the charts in Figs. 8-13, it is easy to determine the safety factor of a rock slope in a transient flow. An example is presented as follows.

A homogeneous rock slope with a height of 20 m and a slope inclination of 45° is considered. The unit weight of the rock mass is 25 kN/m^3, the uniaxial compressive strength is 20 MPa, and the values of the Hoek-Brown indices are $GSI = 30$ and $m_i = 20$. The water table falls 8 m from the crest line with a rate of 0.1 m/d. First, the dimensionless parameter is calculated as $\sigma/\gamma H = 20000/(25 \times 20) = 40$. Then, FOS =3.96 is obtained directly from Fig. 9.

To further evaluate the influences of the properties of the rock mass (GSI and m_i), the hydraulic conditions (L/H and v) and the slope geometry (β) on the stability of rock slopes, a parametric analysis is conducted.

Fig. 14 plots the change in the safety factor against the water level coefficient L/H. L/H has a substantial effect on the slope stability. The safety factor decreases rapidly within $L/H < 0.2$. With the increase of L/H, the variation rule of the safety factor tends to be more gentle and eventually barely changes (or even changes in the opposite direction) when $L/H > 0.6$.

Fig. 14 also illustrates, as discussed earlier, that in some cases the minimum value of the safety factor is attained at $L/H = 0.6$ or 0.8; hence, during the process of groundwater level drawdown, the state of a slope is most susceptible at this moment. The variation rules of FOS with the parameters GSI, m_i, β and v are also shown in Fig. 14. The relationships between FOS and the HB indices, namely, GSI and m_i , exhibit nonlinearity, whereas FOS changes more linearly with the magnitudes of β and v.

8. Conclusions

Based on the discretization-based kinematic analysis, a new approach was proposed for stability analysis of the Hoek-Brown slopes under 'transient' drawdown condition. With the application of the generalized tangent technique and the phreatic surface equation, rigorous solutions of safety factor are obtained via a discretization technique. A set of stability charts was proposed for preliminary design. The conclusions of this study are as follows:

The accuracy of the specified equation in describing the phreatic line within a slope was evaluated by comparing numerical solutions. According to a comparison with previous results, the equation can provide an accurate description of the bent phreatic surface in a transient flow. The utilization of such an equation enables the theoretical analysis of slopes that are subjected to a transient drawdown.

The discretization technique, which has strong applicability and portability, was used to generate the velocity discontinuity surface of the rock slope in this paper. This technique not only guarantees a kinematically admissible velocity field for spatially varying strength but also avoids complicated integrals when dealing with complex phenomena such as water drawdown. Improving the computational efficiency was the reason why we adopted this discretization method in this study.

A set of stability charts for a reservoir rock slope was plotted against the index $SR = \sigma_c/\gamma H$, which is an extension of the current research that is limited to soil slopes under extremely 'rapid' and 'slow' flow scenarios. These charts can be conveniently used to obtain the safety factors of jointed homogeneous rock slopes that are subjected to transient flow conditions, for preliminary estimation. An application example was also presented to demonstrate the chart method.

A parametric analysis of the safety factor was conducted with the variation of the water level. It is found that the most vulnerable status of slopes occurs when the reservoir is fully drained or when the water level is low. This phenomenon is similar to that observed in soil slopes. The analysis also indicates that the strength parameters, namely, *GSI* and m_i, have nonlinear influences on the slope stability, whereas the effects of the geometrical slope parameter β and the water level drop rate v appear to be linear.

References

Bandini, P., Salgado, R. and Loukidis, D. (2003), "Stability of seismically loaded slopes using limit analysis", *Geotechnique*, **53**(5), 463-480. https://doi.org/10.1680/geot.2003.53.5.463.

Berilgen, M.M. (2006), "Investigation of stability of slopes under drawdown conditions", *Comput. Geotech.*, **34**(2), 81-91. https://doi.org/10.1016/j.compgeo.2006.10.004.

Carranza-Torres, C. and Fairhurst, C. (1999), "The elasto-plastic response of underground excavations in rock masses that satisfy the Hoek–Brown failure criterion", *J. Rock Mech. Mining Sci.*, **36**(6), 777-809. https://doi.org/10.1016/s0148-9062(99)00047-9.

Chehade, H.A., Dias, D., Sadek, M., Jenck, O. and Chehade, F. H. (2019), "Seismic analysis of geosynthetic-reinforced retaining wall in cohesive soils", *Geotextiles Geomembr.,* **47**(3), 315-326. https://doi.org/10.1016/j.geotexmem.2019.02.003.

Gaziev, E.G. (2001), "Stability analysis of the rock slope in the zimapan arch dam reservoir, Mexico", *Bulletin Eng. Geology Environ.,* **60**(2), 135-137. https://doi.org/10.1007/s100640000095.

Hoek, E., Carranza-Torres, C. and Corkum, B. (2002) "Hoek-Brown failure criterion-2002 edition", *Proceedings of the Fifth North American Rock Mechanics*, Toronto, Canada, July.

Huang, F. and Yang, X.L. (2010), "Upper bound solutions for the face stability of shallow circular tunnels subjected to nonlinear failure criterion", *Geoshanghai International Conference*, Shanghai, China, May.

Karray, M., Hussien, M.N., Delisle, M.C. and Ledoux, C. (2018), "Framework to assess pseudo-static approach for seismic stability of clayey slopes", *Canadian Geotech. J.*, **55**(4), 1860–1876. https://doi.org/10.1139/cgj-2017-0383.

Khorasani, E., Amini, M., Hossaini, M.F. and Medley, E. (2019), "Evaluating the effects of the inclinations of rock blocks on the stability of bimrock slopes", *Geomech. Eng.,* **17**(3), 281-287. https://doi.org/10.12989/gae.2019.17.3.281.

Lane, P.A. and Griffiths, D.V. (2000). "Assessment of stability of slopes under drawdown conditions", *J. Geotech. Geoenviron. Eng.*, **126**(5), 443-450. https://doi.org/10.1061/(ASCE)1090-0241(2000)126:5(443).

Leshchinsky, B. and Ambauen, S. (2015), "Limit equilibrium and limit analysis: comparison of benchmark slope stability problems", *J. Geotech. Geoenviron. Eng.*, **141**(10). https://doi.org/10.1061/(ASCE)GT.1943-5606.0001347.

Li, A.J., Lyamin, A.V. and Merifield, R.S. (2008). "Seismic rock slope stability charts based on limit analysis methods", *Comput. Geotech.*, **36**(1-2), 135-148. https://doi.org/10.1016/j.compgeo.2008.01.004.

Lu, C.P., Shu, L.C., Chen, X.H. and Cheng, C. (2011). "Parameter estimation for a karst aquifer with unknown thickness using the genetic algorithm method", *Environ. Earth Sciences*, **63**(4), 797-807. https://doi.org/10.1007/s12665-010-0751-8.

Lysandros, P., Elias, G. and Konstantinos-Paraskevas, G. (2020), "Stability assessment of soil slopes in three dimensions: The effect of the width of failure and of tension crack", *Geomech. Eng.,* **22**(4), 319-328. https://doi.org/10.12989/gae.2020.22.4.319.

Merifield, R.S., Lyamin, A.V. and Sloan, S.W. (2006). "Limit analysis solutions for the bearing capacity of rock masses using the generalised hoek-brown criterion", *J. Rock Mech. Mining Sci.*, **43**(6), 920-937. https://doi.org/10.1016/j.ijrmms.2006.02.001.

Mollon, G., Phoon, K.K., Dias, D. and Soubra, A.H. (2011), "Validation of a new 2D failure mechanism for the stability analysis of a pressurized tunnel face in a spatially varying sand", *J. Eng. Mech.*, **137**(1), 8-21. https://doi.org/10.1061/(ASCE)EM.1943-7889.0000196.

Nadukuru, S.S. and Michalowski, R.L. (2013). "Three-dimensional displacement analysis of slopes subjected to seismic loads", *Canadian Geotech. J.*, **50**(6), 650-661. https://doi.org/10.1139/cgj-2012-0223.

Rutqvist, J., Stephansson, O. (2003). "The role of hydromechanical coupling in fractured rock engineering", *Hydrogeology Journal*, **11**(1), 7-40. https://doi.org/10.1007/s10040-002-0241-5.

Saada, Z., Maghous, S. and Garnier, D. (2012). "Stability analysis of rock slopes subjected to seepage forces using the modified hoek-brown criterion", *J. Rock Mech. Mining Sci.*, **55**, 45-54. https://doi.org/10.1016/j.ijrmms.2012.06.010.

Sahoo, P.P. and Shukla, S.K. (2019), "Taylor's slope stability chart for combined effects of horizontal and vertical seismic coefficients", *Géotechnique*, **69**(4), 344-354. https://doi.org/10.1680/jgeot.17.p.222.

Sun, Z.B., Li, J.F., Pan, Q.J., Dias, D., Li, S.Q. and Hou, C.Q. (2018), "Discrete kinematic mechanism for nonhomogeneous slopes and its application", *J. Geomech.*, **18**(12), 04018171. https://doi.org/10.1061/(ASCE)GM.1943-5622.0001303.

Tiwari, G. and Latha, G.M. (2017), "Reliability analysis of jointed rock slope considering uncertainty in peak and residual strength parameters", *Bulletin Eng. Geology Environ.*, **78**, 913-930 https://doi.org/10.1007/s10064-017-1141-1.

Ukritchon, B. and Keawsawasvong, S. (2018), "Stability of unlined square tunnels in hoek-brown rock masses based on lower bound analysis", *Comput. Geotech.*, **105**(1), 249-264. https://doi.org/10.1016/j.compgeo.2018.10.006.

Viratjandr, C. and Michalowski, R.L. (2006), "Limit analysis of submerged slopes subjected to water drawdown", *Canadian Geotech. J.*, **43**(8), 802-814. https://doi.org/10.1139/T06-042.

Yang, X.L. and Zou, Z.F. (2006). "Stability factors for rock slopes subjected to pore water pressure based on the Hoek-Brown failure criterion", *J. Rock Mech. Mining Sci.*, **43**(7), 1146-1152. https://doi.org/10.1016/j.ijrmms.2006.03.010.

Younger, P.L. and Elliot, T. (1995), "Chalk fracture system characteristics: implications for flow and solute transport", *Quarterly J. Eng. Geology Hydrogeology*, **28**(Supplement 1), S39-S50. https://doi.org/10.1144/gsl.qjegh.1995.028.s1.04.

Zheng, Y.R., Shi, W.M. and Kong, W.X. (2004). "Calculation of seepage forces and phreatic surface under drawdown conditions", *Chinese J. Rock Mech. Eng.*, **66**(21), 2524-2533. https://doi.org/1000-6915(2004)18-3203-08.